NACA

RESEARCH MEMORANDUM

HEAT TRANSFER MEASURED ON A FLAT-FACE CYLINDER IN

FREE FLIGHT AT MACH NUMBERS UP TO 13.9

By William E. Stoney, Jr., and Andrew G. Swanson

Langley Aeronautical Laboratory
Langley Field, Va.

Declassified June 5, 1962

NATIONAL ADVISORY COMMITTEE
FOR AERONAUTICS
WASHINGTON
June 17, 1957

NATIONAL ADVISORY COMMITTEE FOR AERONAUTICS

RESEARCH MEMORANDUM

HEAT TRANSFER MEASURED ON A FLAT-FACE CYLINDER IN

FREE FLIGHT AT MACH NUMBERS UP TO 13.9

By William E. Stoney, Jr., and Andrew G. Swanson

SUMMARY

A five-stage rocket model was flown to a Mach number of 13.9 and free-stream Reynolds number based on nose diameter of 1.6×10^6 at an altitude of 81,500 feet. Temperatures were measured at 12 stations on the front and sides of its flat-face copper nose. Heating rates calculated from the temperature time histories are compared with theoretical predictions of these rates. The stagnation heating rates agreed well with calculations which included estimates of real gas effects, and it appeared that no large transfer due to radiation was present.

INTRODUCTION

With the advent of hypersonic flight by missiles (and soon, perhaps, by aircraft), the phenomena associated with the aerodynamic heating of such bodies have become of prime importance. The noses of such bodies are usually the critical areas, and it has become apparent that some degree of bluntness must always be used to withstand the high heating rates of this flight regime. The perfectly flat nose is an extreme case of bluntness. For a given diameter it has lower heat-transfer rates at the stagnation point than any other shape (although the local rates rise toward the corners), and there is evidence that such extreme bluntness is favorable to longer runs of laminar flow. For these reasons a perfectly flat copper nose of 5-inch diameter was tested in free flight at the Langley Pilotless Aircraft Research Station at Wallops Island, Va., at Mach numbers up to 13.9 and an altitude of 81,500 feet. The results are compared herein with available appropriate theoretical calculations.

The flight of this model is also interesting from the point of view of its overall design and performance. The model serves as an example of a reentry missile $\left(\dfrac{W}{C_D S} = 200 \text{ lb/sq ft}\right)$ with a maximum reentry velocity

of about 13,600 feet per second, a reentry angle of $-5°$, and an impact Mach number of about 0.4.

The fourth-stage rocket motor (JATO 1.52-KS-33, 550, XM19 (Recruit)) used in the present investigation was made available by the U. S. Air Force.

SYMBOLS

A_{n+1} cross-sectional area between elements n and $n+1$

A_{n-1} cross-sectional area between elements n and $n-1$

a_0 speed of sound at stagnation point

C_D drag coefficient

C_H heat-transfer coefficient, $\dfrac{q}{\rho_l c_{p,l} U_l} \dfrac{1}{T_0 - T_w}$

c_p heat capacity

D diameter

D_{12} coefficient of diffusion between atoms and molecules

h enthalpy

k conductivity

l distance along surface of nose measured from center line

Δl_{n+1} distance between thermocouple locations of elements n and $n+1$

Δl_{n-1} distance between thermocouple locations of elements n and $n-1$

M Mach number

N_{Le} Lewis number, $\dfrac{\rho D_{12} c_p}{k}$

N_{Nu} Nusselt number, $\dfrac{q l c_{p,w}}{k_w \left(h_t - h_w \right)}$

N_{Pr} Prandtl number

P pressure

q heating rate, Btu/(sec)(sq ft)

q' apparent heating rate, $\rho_c c_{p,c} \tau_c \dfrac{dT}{dt}$

$\dfrac{q_{o,f}}{q_{o,h}}$ ratio of stagnation heating rate on flat face to stagnation heating rate on hemisphere of equal diameter

R Reynolds number

$R_l \equiv \dfrac{\rho_l U_l l}{\mu_l}$

$R_w \equiv \dfrac{U_l l \rho_w}{\mu_w} = \left[\left(\dfrac{dU}{dx} \right)_o l^2 \dfrac{\rho_w}{\mu_w} \text{ at stagnation point} \right]$

r radius of nose, 2.5 in.

S frontal area of body

S_n surface area exposed to airstream of element n

T temperature, $^\circ F$

t time, sec

U velocity

W weight

x horizontal range, ft

z altitude, ft

μ viscosity

ρ density

τ thickness

Subscripts:

c   copper wall

d   based on diameter

f   flat face

h   hemisphere

l local, outside boundary layer

o   at stagnation point

t   total

w   air at temperature of wall

∞ free stream

MODEL AND TEST

Model

The model was propelled by a five-stage rocket system: the first stage consisted of an M6 JATO "Honest John" rocket motor; the second and third stages, M5 JATO "Nike" rocket motors; the fourth stage, a JATO, 1.52-KS-33, 550, XM19 "Recruit" rocket motor; and the fifth stage, a JATO, 1.3-KS-4800, T55 rocket motor. A photograph of the complete assembly mounted on the launcher just prior to firing is shown in figure 1. Figure 2 presents a sketch of the five stages together with a table presenting the weights of the various components.

A photograph of the model alone is presented in figure 3. Details of the nose construction and thermocouple installation and locations are shown in figure 4. The thermocouples were no. 30 gage platinum-rhodium wires beaded together in a ball which was peened into a small hole on the inner surface of the copper nose. No special care was taken with the finish of the surface, and it is estimated that the roughness was of the order of 60 microinches.

Test

The model was launched at an angle of 73° with the horizontal and followed the flight path shown in figure 5. Up to the firing of the

third stage the information in figure 5 was obtained directly from tracking the model with an NACA modified SCR-584 radar unit. After this point it was necessary to correct the radar data through use of velocities obtained by integrating the time histories of two longitudinal accelerometers mounted inside the model. Near burnout of the last stage the radar lost the model completely, and the flight path after this point was calculated by use of the integrated velocities alone. After 94 seconds the flight path shown is the result of calculations alone since the decelerations, although measured all the way to splash, were too inaccurate to be used because of their low values. The complete flight path is shown in the small curve in figure 5.

Because of accuracy limitations useful heating data could be obtained only for relatively high heat-transfer rates which occurred during the time period from 88 to 94 seconds; thus the flight conditions are presented in more detail for these times only. Figure 6 presents the velocity and altitude history of the model for this time period. As mentioned previously the velocities were obtained from adding integrated accelerometer values to the velocity obtained from the radar data at its last reliable velocity point, which was just before firing of the third-stage motor. Since a continuous error of 1 percent in the accelerometer readings would introduce an error of approximately ±400 feet per second in the peak velocity value, a possibility of errors of this magnitude must be considered. This possible spread is noted in the figures presenting velocity, Mach number, and calculated heating rates. The values of velocity and altitude of figure 6 were combined with radiosonde values of density and temperature to obtain the values of M and $R_{\infty,D}$ shown in figure 7.

DATA REDUCTION

The basic data of this test are the temperature measurements. The temperature time histories for thermocouples 1 and 8 are presented in figure 8. The actual data points are circled. The filled circles represent points neglected in the fairing because of noise in the original data. The solid lines are those which were faired through the data by hand and French curve and which were used in the calculation of the local heating rates. These stations are typical of the front (thermocouple 1) and side (thermocouple 8) temperature time histories. Table I presents the values of the temperatures from these faired curves for all stations. The table has been continued for times beyond 94 seconds to a time well past that at which peak temperature occurred at the front surface stations. The values for times beyond 94 seconds were faired from plots having smaller scales than those used for the earlier times and thus may not be as reliable. This table has been included to enable the reader to check his own temperature calculation methods with the data of this flight.

The slopes of these faired curves were read at 0.2-second intervals, and the resulting values were plotted and examined for obvious scatter in the values. The values of the slopes were then used in the equation

$$q' = \rho_c c_{p,c} \tau_c \frac{\partial T}{\partial t} \tag{1}$$

to calculate the apparent heating rate q' for each of the measured points. These apparent heating rates are shown by the dashed lines of figure 9. Internal and external radiation heating rates were so low as to be completely negligible during the period for which the heating rates were calculated. Temperature gradients in the skin normal to the surface were also neglected. Calculations for the effect of these gradients by a one-dimensional heat-flow analysis did little more than add scatter to the heating rates obtained by equation (1), which assumes constant temperature through the wall. These same calculations indicated a 40° difference between front and rear surface temperatures (at thermocouple 1) at the time of maximum heating.

The heating rates calculated by equation (1) are called "apparent" because of the existence of fairly large lateral heat flows in the skin caused by the lateral temperature gradients in the skin. The magnitude of these temperature gradients may be seen from the plots of temperature as a function of position presented in figure 10. The 97-second line shows the temperature distribution for the time of the maximum temperatures recorded.

The calculation of the lateral heating rates was made by the following method. The nose was divided into pie-shaped elements, one for each thermocouple position, and the temperature of each element was assumed to be that of the attached thermocouple:
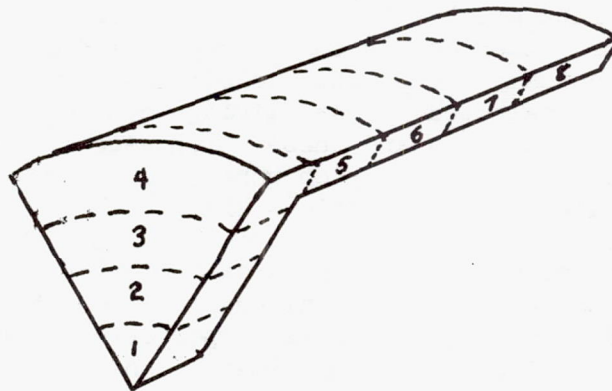
The following difference equation was used to calculate the real aerodynamic heat input to the element n under consideration:

$$q_n = \rho_c c_{p,c} \tau_c \frac{dT_n}{dt} + \frac{kA_{n+1}}{S_n} \frac{(T_n - T_{n+1})}{\Delta l_{n+1}} + \frac{kA_{n-1}}{S_n} \frac{(T_n - T_{n-1})}{\Delta l_{n-1}} \qquad (2)$$

Equation (2) is an approximate method; however, because temperatures were measured at only a few points, this method was considered to be better than an attempt to calculate heating rates by obtaining $\frac{dT}{dx}$ and $\frac{d^2T}{dx^2}$ from the data and using the differential forms of the equation. The results of these calculations are the solid lines of figure 9. No attempt was made to calculate the values for thermocouple 4 (corner) since the high temperature gradient between thermocouples 4 and 5 made any accuracy in this region out of the question.

ACCURACY

The accuracy of telemeter and readout process is considered to be within ±2 percent of the full-scale value of any quantity. Thus the temperatures are considered to be accurate within ±20° although, as the plot of figure 8 shows, the scatter about the faired line is much less than this value. The values of q' are felt to be within ±5 percent. The accuracy of the correction due to skin heat conduction is unknown; however, for thermocouples 1, 2, 7, and 8, where the correction is small, large errors in it would be negligible. As mentioned previously, the possible errors in the correction for station 4 were so large as to make it useless.

An estimation of the overall accuracy of the data can be made by comparisons of data for which the prime variables are supposedly constant. This type of comparison does not of course eliminate the possibility of systematic error in the measurements but only indicates its randomness or repeatability. Such a comparison is shown in figure 11 for two sets of thermocouples located on the face of the model at $l/r = 0.4$ and 0.8. These data were corrected for conduction as described previously (the temperatures at station 4 were used in the corrections for both thermocouples 10 and 12 as well as for thermocouple 3). The differences are believed to be real, that is, they are obvious even in the temperature-time plots, and are not merely the result of inaccuracies in fairing or computing. They may be the result of aerodynamic differences caused by rolling or the slight pitching motion of the model. Although the roll rate is not known, the normal and transverse accelerometers showed an oscillation during the test period of about ±3g. If the lift-curve slope is assumed to be linear near zero angle of attack, this oscillation could be due to an angular oscillation of about $\pm1\frac{1}{2}°$.

Some unpublished data from the Ames supersonic free-flight wind tunnel

have indicated that blunt-nose flare-stabilized bodies such as the present test vehicle are unstable at small angles of attack, and if this is the case it would be difficult to say exactly what angles the measured transverse accelerations represent. Perhaps the important conclusion to be drawn from the comparisons of figure 11 is that the order of repeatability of the heating rates is ±25 Btu/(sec)(sq ft). This, of course, makes comparisons of low heating rates with theory of little value, for example, those on the front surface before 89 seconds. Note in figure 9 that the peaks and valleys in the low heating rates measured on the side thermocouples are of this same order, ±25 Btu/(sec)(sq ft).

Another source of error was present in unknown amount because of the heat flow into the Micarta block which had been found necessary for the high temperature loads expected. Calculations by a one-dimensional heat-flow method, in which the measured temperature history of thermocouple 1 was assumed to exist on the surface of the Micarta, showed a negligible amount of heat loss to this source. The actual measurements were made in the center of $\frac{1}{4}$-inch holes in the Micarta. However, relatively crude tests made by pressing Micarta blocks against a strip of stainless steel (in this case there was no hole around the wire) and heating the steel to simulate the temperature-time histories of the flight indicated that as much as 30 or 60 Btu/(sec)(sq ft) might be lost to the Micarta. A process such as sublimation or boiling of the Micarta would have to be present to explain the difference between the calculated and measured loss values.

RESULTS AND DISCUSSION

Comparison of Measured and Theoretical and Stagnation-Point

Heating Rates

The measured heating rates (corrected for lateral conduction) for thermocouple 1 are compared in figure 12 with theoretical predictions based on the method of Fay and Riddell (ref. 1). This method assumes equilibrium conditions in the boundary layer and includes values for air under these conditions from National Bureau of Standards computations. Their results may be expressed by the following equation:

$$q = \frac{N_{Nu}}{\sqrt{R_w}} \frac{\sqrt{\rho_w \mu_w \left(\frac{dU}{dx}\right)_o}}{N_{Pr}} \left(h_t - h_w\right)$$

where

$$\frac{N_{Nu}}{\sqrt{R_w}} = 0.67 \left(\frac{\rho_o \mu_o}{\rho_w \mu_w}\right)^{0.4} \quad \text{for} \quad N_{Le} = 1 \quad \text{and} \quad N_{Pr} = 0.71$$

The evaluation of the temperature and viscosity was made by assuming ideal gas (constant c_p) conditions behind the normal shock. This assumption avoids the problems associated with determining the properties in the dissociated flow outside the boundary layer. In order to be consistent the equilibrium dissociation values of $\rho\mu$ used in the calculations of reference 1 should be used here also. The heating rates calculated by using the $\rho\mu$ values of reference 1 (fig. 1 of ref. 1) are only 2 to 3 percent higher than those calculated by using the ideal gas conditions.

A value of $\sqrt{\left(\frac{dU}{dx}\right)_o}$ of the flat face equal to $0.5\sqrt{\left(\frac{dU}{dx}\right)_o}$ for a

hemisphere of equal diameter was used $\left(\left(\frac{dU}{dx}\right)_{o,h} = \frac{1}{r}\sqrt{2\frac{P_o}{\rho_o}}\right.$ from Newtonian

flow$\Big)$. This value of $\frac{q_{o,f}}{q_{o,h}} = 0.5$ was obtained by assuming the quantity

$\frac{r}{a_o}\left(\frac{dU}{dx}\right)_o$ = Constant with Mach number. The details of this calculation

are presented in the appendix. The band of uncertainty in the theory due to uncertainty in the velocity measurements is indicated in figure 12 for the maximum Mach number. Since the uncertainty in the theory is due to uncertainty in velocity alone and is proportional to the square of the velocity, the error would be considerably less for the earlier or later times.

The difference between experimental and theoretical values is small and the agreement is especially good for the high heating rates where the experimental accuracy is best. The fact that the experimental values are always below the theoretical values indicated that no large unknown sources of heat transfer (by radiation of the gas layer, for example) occurred.

Comparison of Measured and Theoretical Heating Rates

Over Entire Front and Side of Nose

No solutions exist which include directly the effects of equilibrium dissociation in the boundary layer for points other than the stagnation

point. It is possible (and easier) to calculate the ratios of local
heating rate to the heating rate at the stagnation point and to use these
ratios with the stagnation-point solution to obtain the values at places
other than the stagnation point. Such methods do not, of course, account
for the changes in state of the air about the body due to the changes in
local temperature and pressure conditions and due to the effects of the
finite relaxation times of the gases. These methods are the best avail-
able at the present time, however; two (refs. 2 and 3) are used for the
face and another for the sides (ref. 4). Comparison of the data on the
basis of ratios of local to stagnation heating rate has the added advan-
tage of eliminating Mach number as an important variable.

These comparisons are shown in figure 13. All the local experi-
mental values are presented as ratios of the experimental stagnation-
point heating rates. On the face the local theoretical values were
divided by the stagnation-point theoretical values. On the sides the
local theoretical values were divided by measured stagnation-point val-
ues, since the calculations for the local heating rates on the sides do
not inherently have a stagnation value connected with them, and the use
of measured stagnation values allows a more direct comparison of the
calculated and measured local values.

The data obtained on the front surface are compared with values
calculated by two theories. These theories differ mainly in that Lees'
results (ref. 2) are functions of local pressure but are not functions
of pressure gradient directly as are the transformations used by Stine
and Wanlass (ref. 3). It should be noted that both of these methods
assume that $\rho\mu$ is constant across the boundary layer. Fay and Riddell
in reference 1 have shown that at the higher speeds $\rho\mu$ varies consider-
ably across the boundary layer, and it is this variation which causes the
drop in $\dfrac{N_{Nu}}{\sqrt{R_w}}$ with increasing velocity. Presentation of the local theo-
retical heating rates as ratios with the stagnation-point rates may
eliminate or at least reduce the effects of this approximation in the
theories of references 2 and 3 when applied to these higher Mach numbers.

The results of both theories are no better than the pressure dis-
tributions which are used with them. The pressure distribution for both
curves labeled M = 1.5 is that calculated by Maccoll and Codd (ref. 5).
(See appendix.) The pressures for the curve labeled M = 5 were esti-
mated from unpublished wind-tunnel data obtained by Morton Cooper of the
Langley Gas Dynamics Branch. The pressures used for calculations at a
Mach number of 5 must be considered to be preliminary in nature. The
heat-transfer coefficients obtained from them are presented only to
indicate the probable effect of Mach number on flat-face heat transfer.

It is apparent that the scatter in the data is such that no definite preference can be said to be shown any of the theoretical curves. However, the general distribution of the heating rates appears to follow the trend shown by all the theories, especially near the maximum Mach number, where the best accuracy in the data can be expected. It is reasonably certain that laminar flow was present on the face at all times during the flight.

The data on the sides are compared with values calculated by laminar flat-plate theory $\left(C_H \sqrt{R_l} = 0.4, \text{ ref. } 4\right)$ with the assumptions that the local conditions were such that the pressure all along the sides was equal to free-stream pressure and that the flow adjacent to the boundary layer had passed through a normal shock. The assumption of constant free-stream pressure on the side of the nose is questionable since over-expansion to pressures lower than stream pressure has been the experience at lower Mach numbers. While percentagewise the comparison between the theoretical or measured values appears to be only fair, actually in terms of the numerical values of heating rates it is usable for most engineering purposes. In spite of the scatter the data appear to follow the trend of decreasing heating-rate ratios with increasing Mach number.

Although the data are compared with laminar calculations there is no real assurance other than the very low local Reynolds numbers $\left(0.01 \times 10^6 < R_l < 0.1 \times 10^6\right)$ involved that the flow remained laminar. In fact, if the turbulent-theory curves of reference 4 are stretched a bit in the cool-wall direction, the values of turbulent C_H obtained are only from 10 to 100 percent higher than the laminar calculations. (See fig. 13.) This spread, when compared with the spread in the data points, is not enough to permit any conclusions to be drawn.

General

The flight of this model is interesting from the point of view of its overall design and performance. It serves as an example of a reentry missile $\left(\dfrac{W}{C_D S} = 200 \text{ lb/sq ft}\right)$ with a maximum reentry velocity of about 13,600 feet per second and a reentry angle of $-5°$. Extended trajectory calculations indicated an impact Mach number of about 0.4. The telemeter signal from the model was good all the way to splash, and the instruments indicated that the model was intact at this time. The temperatures at four stations are presented all the way to splash in figure 14 together with calculated values of altitude and Mach number.

The temperature histories presented in figure 10 and figure 14 show the effectiveness of the sides as a heat sink, since the corners, which were probably receiving the highest heating rates, did not reach the highest temperatures. This was, of course, the result of the extremely low heating rates experienced on the sides as well as the high conductivity of copper. As noted previously, these low rates were apparently not dependent on the character of the boundary-layer flow because at these low local Reynolds numbers both the turbulent and the laminar heating rates were similar.

CONCLUSIONS

A five-stage rocket model was flown to a maximum Mach number of 13.9 at an altitude of 81,500 feet. Temperature time histories were taken at 12 stations located on the front and sides of its flat-face copper nose. Comparison of the heating rates derived from these temperature histories with theoretical calculations indicate the following two conclusions:

1. The measured stagnation heating rates agreed well with the rates calculated for equilibrium conditions by a method which included estimations of real gas effects. It appears that no large effects due to radiation from the gas layer were present.

2. Comparison of theoretical and measured values of the ratios of local heating rates to stagnation-point heating rates showed reasonable agreement over the front surface. On the sides the crude assumption of local pressure equal to free-stream pressure gave poor agreement percentagewise; however, because of the low rates involved the absolute agreement was good enough for most engineering purposes.

Langley Aeronautical Laboratory,
    National Advisory Committee for Aeronautics,
        Langley Field, Va., April 17, 1957.

APPENDIX

PRESSURE DISTRIBUTIONS ON FLAT FACE

Since the calculations of heating rates can be no better than the accuracy of the local conditions on which they are based, a plot of the values used in this report is presented in figure 15. The curve of Maccoll and Codd (ref. 5) for $M = 1.5$ calculated by a method employing successive approximations was used to calculate the heat-transfer rates. Recently tests were made in the preflight jet at the Langley Pilotless Aircraft Research Station at Wallops Island, Va., at a Mach number of 2, and a curve faired from these pressures is presented as a comparison.

Even more recent tests by Morton Cooper of the Langley Gas Dynamics Branch showed somewhat higher pressures (for example, $P/P_O = 0.88$ to 0.92 at $l/r = 0.9$), and a curve faired through these data was used in the calculation by the method of Stine and Wanlass (labeled $M = 5$ in fig. 13). As mentioned in the text this calculation was made only as an indication of the heat-transfer trend with increasing Mach number.

Although the rate of change of velocity at the stagnation point is difficult to compute accurately from pressure distributions alone, the value obtained from the Maccoll and Codd distribution $\left(\frac{r}{a_O}\left(\frac{dU}{dx}\right)_O = 0.3\right)$ gives a ratio of $\frac{q_{o,f}}{q_{o,h}}$ of 0.55 at $M = 1.5$. This value can be compared with the inviscid flow value of 0.65 obtained by Probstein (ref. 6). If it is assumed that the expression $\frac{r}{a_O}\left(\frac{dU}{dx}\right)_O = 0.3$ is invariant with Mach number, this ratio of $\frac{q_{o,f}}{q_{o,h}}$ decreases with Mach number and reaches a limit of about 0.5 for Mach numbers above 4 (see fig. 16). For $\frac{r}{a_O}\left(\frac{dU}{dx}\right)_O$ to remain invariant means that the value of $\frac{P}{P_O}$ near the stagnation point is constant with Mach number also. Although the variations of $\frac{P}{P_O}$ between the $M = 5$, 2, and 1.5 values are small and the measurement accuracy is of nearly the same magnitude, it is noteworthy that the ratio $\frac{P}{P_O}$ increases with Mach number. This increase of $\frac{P}{P_O}$ with Mach number is most prominent at l/r near the edge. Such an increase at the edge, however, could be taken to mean that the values closer to the stagnation point increased with Mach number also. Even a small increase

in $\dfrac{P}{P_O}$ near the stagnation point would decrease $\dfrac{r}{a_O}\left(\dfrac{dU}{dx}\right)_O$ at the stag-

nation point, which would indicate a reduction in $\dfrac{q_{O,f}}{q_{O,h}}$ even greater

than that shown in figure 16(b). For this reason it appears probable
that the theoretical heating rates calculated by using the ratio of
$\dfrac{q_{O,f}}{q_{O,h}} = 0.5$ are either correct of slightly too high. This invariance

of $\dfrac{r}{a_O}\left(\dfrac{dU}{dx}\right)_O$ (or actually slight increase) is opposed to the variation

commonly used for hypersonic flows, namely, $\dfrac{c_p}{c_{p,O}} = $ Constant. This

relation predicts a decrease in values of $\dfrac{P}{P_O}$ with increasing Mach

number.

REFERENCES

1. Fay, J. A., and Riddell, F. R.: Stagnation Point Heat Transfer in
   Dissociated Air. Res. Note 18, AVCO Res. Lab., June 1956.

2. Lees, Lester: Laminar Heat Transfer Over Blunt-Nosed Bodies at
   Hypersonic Flight Speeds. Jet Propulsion, vol. 26, no. 4,
   Apr. 1956, pp. 259-269.

3. Stine, Howard A., and Wanlass, Kent: Theoretical and Experimental
   Investigation of Aerodynamic Heating and Isothermal Heat-Transfer
   Parameters on a Hemispherical Nose With Laminar Boundary Layer at
   Supersonic Mach Numbers. NACA TN 3344, 1954.

4. Van Driest, E. R.: The Problem of Aerodynamic Heating. Aero. Eng.
   Rev., vol. 15, no. 10, Oct. 1956, pp. 26-41.

5. Maccoll, J. W., and Codd, J.: Theoretical Investigation of the Flow
   Around Various Bodies in the Sonic Region of Velocities. British
   Theoretical Res. Rep. No. 17/45, B.A.R.C. 45/19, Ministry of Supply,
   Armament Res. Dept., 1945.

6. Probstein, Ronald F.: Inviscid Flow in the Stagnation Point Region
   of Very Blunt-Nosed Bodies at Hypersonic Flight Speeds. WADC
   TN56-395 (Contract No. AF 33(616)-2798), Wright Air Dev. Center,
   U. S. Air Force, Sept. 1956. (Also available from ASTIA as Doc.
   No. AD97273.)

TABLE I

FAIRED TEMPERATURE VALUES

| Time, sec	Temperature, °F, at station -											
	1	2	3	4	5	6	7	8	9	10	11	12
88.0	190	192	202	190	155	148	149	152	193	200	197	189
88.2	200	205	225	215	165	160	156	160	204	215	217	194
88.4	213	220	251	237	176	171	165	165	221	236	240	205
88.6	232	245	285	265	189	182	175	173	247	265	267	226
88.8	260	282	324	295	203	190	187	180	279	300	297	253
89.0	294	324	370	330	216	200	200	190	314	340	327	286
89.2	335	367	424	370	230	208	214	198	355	387	365	330
89.4	383	417	481	420	245	218	229	208	402	440	405	381
89.6	440	475	545	475	268	230	244	220	453	500	450	440
89.8	505	537	621	535	288	245	257	232	515	565	505	510
90.0	580	610	706	600	307	262	271	245	588	644	570	590
90.2	664	695	795	665	335	280	284	260	672	735	652	687
90.4	751	785	886	738	367	297	297	275	762	840	755	794
90.6	842	870	977	810	400	315	310	290	849	948	860	900
90.8	925	955	1063	880	437	335	321	305	933	1048	960	1005
91.0	1000	1040	1140	945	475	355	333	318	1014	1142	1055	1108
91.2	1075	1120	1212	1005	515	375	345	330	1093	1240	1145	1205
91.4	1147	1190	1273	1060	555	395	355	343	1168	1305	1220	1291
91.6	1212	1245	1325	1105	592	415	365	355	1240	1362	1284	1364
91.8	1273	1295	1369	1145	627	434	376	365	1305	1408	1343	1419
92.0	1326	1337	1404	1180	660	454	383	375	1368	1445	1398	1462
92.2	1375	1375	1431	1205	668	473	395	382	1415	1480	1450	1492
92.4	1416	1415	1458	1230	713	492	403	388	1459	1505	1495	1513
92.6	1452	1448	1471	1250	735	513	410	395	1496	1530	1530	1532
92.8	1485	1480	1487	1268	758	533	418	400	1528	1555	1560	1552
93.0	1516	1507	1503	1285	778	553	425	405	1557	1575	1585	1570
93.2	1545	1535	1516	1303	806	573	434	412	1585	1593	1610	1590
93.4	1574	1560	1530	1320	839	594	448	427	1610	1612	1633	1610
93.6	1600	1585	1542	1335	865	615	465	443	1633	1630	1655	1630
93.8	1625	1605	1555	1353	887	637	477	452	1656	1645	1677	1649
94.0	1650	1625	1566	1370	909	658	488	460	1676	1660	1700	1668
94.5	1700	1675	1590	1400	970	710	520	485	1728	1680	1750	1700
95.0	1740	1710	1610	1430	1020	760	550	506	1760	1700	1780	1720
95.5	1770	1732	1620	1448	1060	800	580	526	1790	1710	1800	1730
96.0	1790	1742	1625	1458	1100	842	600	540	1806	1713	1815	1730
96.5	1800	1750	1622	1462	1130	880	625	560	1809	1710	1820	1730
97.0	1808	1750	1618	1468	1155	910	650	575	1808	1700	1820	1720
97.5	1805	1742	1610	1468	1180	940	670	590	1800	1690	1810	1710
98.0	1800	1736	1600	1468	1198	962	692	610	1790	1680	1802	1700
98.5	1790	1726	1590	1468	1210	988	715	621	1780	1663	1797	1690
99.0	1780	1710	1580	1468	1220	1007	735	633	1770	1650	1781	1678
99.5	1770	1700	1570	1460	1232	1020	755	650	1760	1632	1770	1660
100.0	1760	1685	1553	1450	1240	1036	772	660	1745	1620	1752	1650
100.5	1748	1670	1540	1442	1250	1050	790	670	1732	1608	1735	1632
101.0	1733	1655	1530	1440	1253	1062	810	682	1720	1591	1720	1620
101.5	1720	1640	1520	1430	1260	1080	825	694	1700	1580	1700	1610
102.0	1700	1623	1510	1422	1262	1090	840	702	1685	1568	1685	1592
102.5	1689	1610	1500	1416	1268	1100	850	710	1668	1550	1668	1578
103.0	1675	1590	1488	1408	1270	1102	860	718	1650	1540	1650	1560
103.5	1658	1575	1475	1400	1270	1110	870	722	1630	1520	1630	1550
104.0	1640	1560	1462	1390	1270	1111	880	730	1613	1510	1614	1532
104.5	1624	1542	1450	1380	1270	1115	888	735	1598	1494	1596	1520
105.0	1610	1527	1440	1370	1268	1118	892	745	1580	1480	1578	1505
105.5	1590	1510	1428	1362	1263	1119	900	750	1562	1465	1560	1488
106.0	1574	1495	1417	1351	1260	1120	908	754	1550	1450	1540	1470
106.5	1555	1480	1402	1342	1258	1120	910	758	1535	1440	1525	1460
107.0	1535	1468	1390	1332	1252	1120	918	762	1517	1420	1508	1445
107.5	1520	1453	1378	1323	1250	1118	920	768	1500	1410	1490	1430
108.0	1500	1440	1363	1313	1242	1115	923	770	1478	1395	1472	1420
108.5	1486	1425	1350	1301	1240	1115	928	773	1470	1380	1460	1410
109.0	1470	1410	1340	1290	1234	1115	930	780	1456	1370	1440	1393
109.5	1450	1400	1330	1280	1230	1110	935	782	1440	1360	1430	1380
110.0	1435	1380	1320	1270	1225	1110	940	788	1420	1348	1410	1370
Measured thickness, in. . . .	0.188	0.188	0.187	----	0.127	0.127	0.127	0.127	0.188	0.188	0.187	0.188
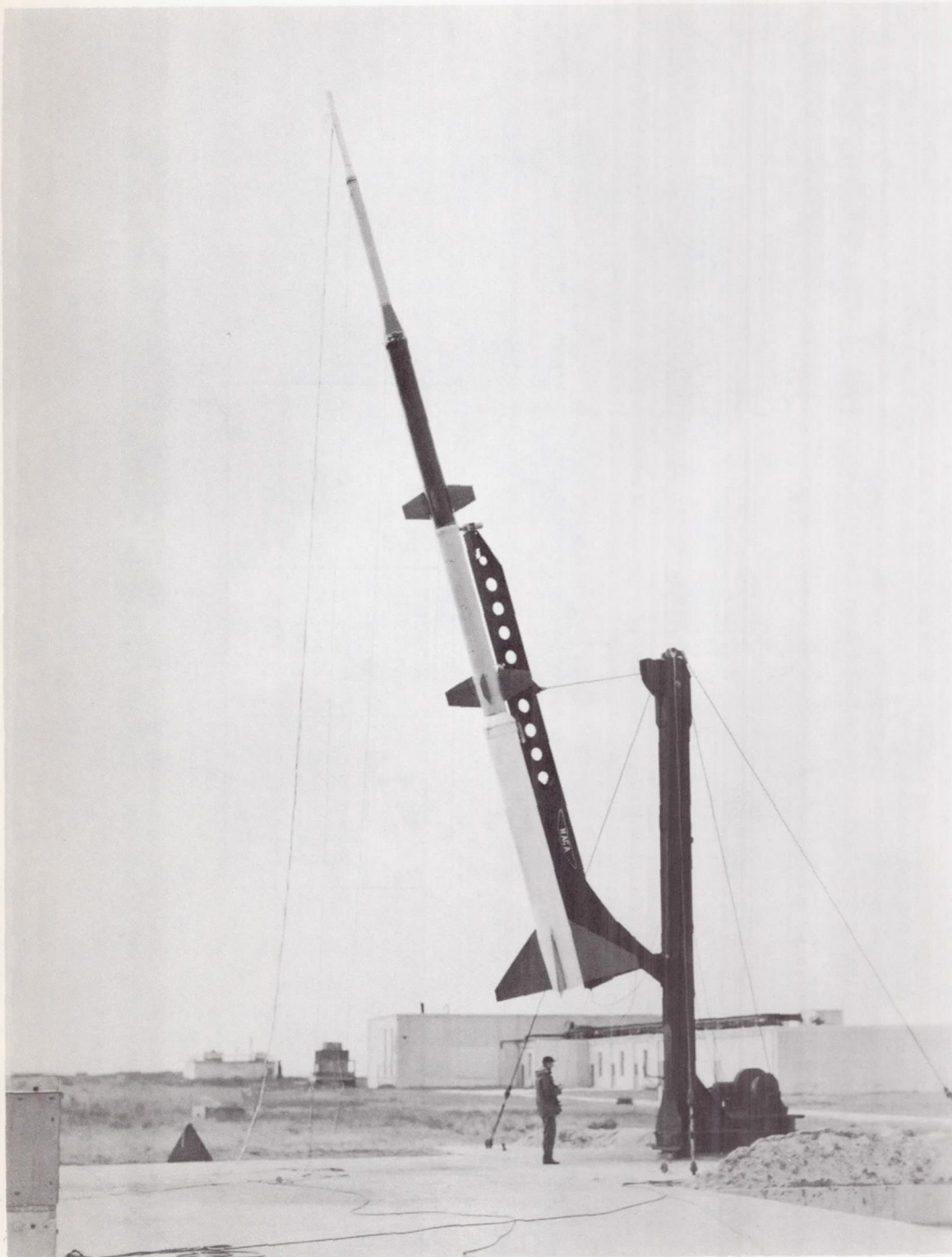
Figure 1.- Five-stage rocket model on launcher.   L-97232

T55	Recruit	Nike	Nike	Honest John
0"	63"	178"	317"	455"	656"
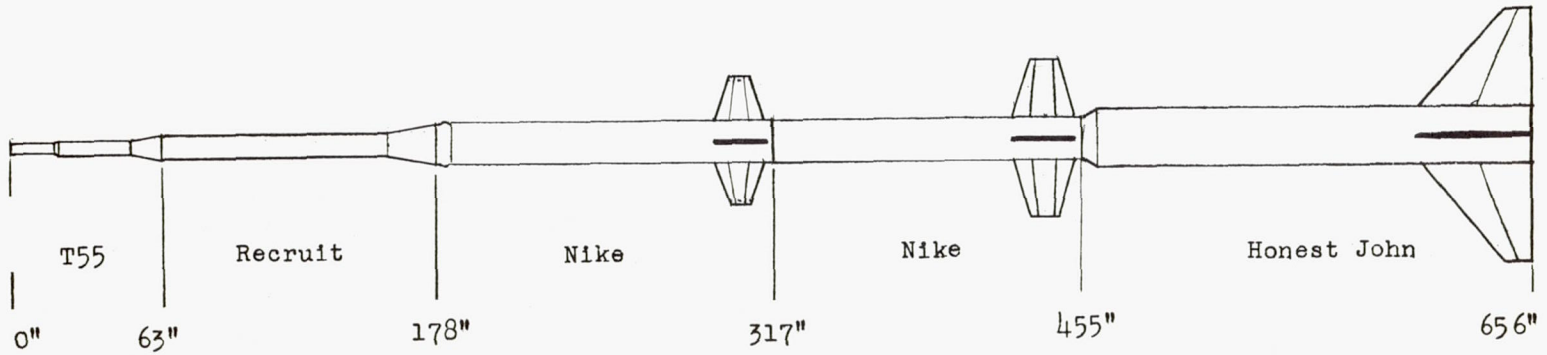
Motor	Weight loaded, lb	Total weight before firing of stage, lb
Honest John	4,120	7,204
Nike	1,310	3,084
Nike	1,309	1,774
Recruit	391	465
[a]T55	74	-----

[a]Weight empty, 39.5 lb

Figure 2.- Assembly of five-stage rocket model.
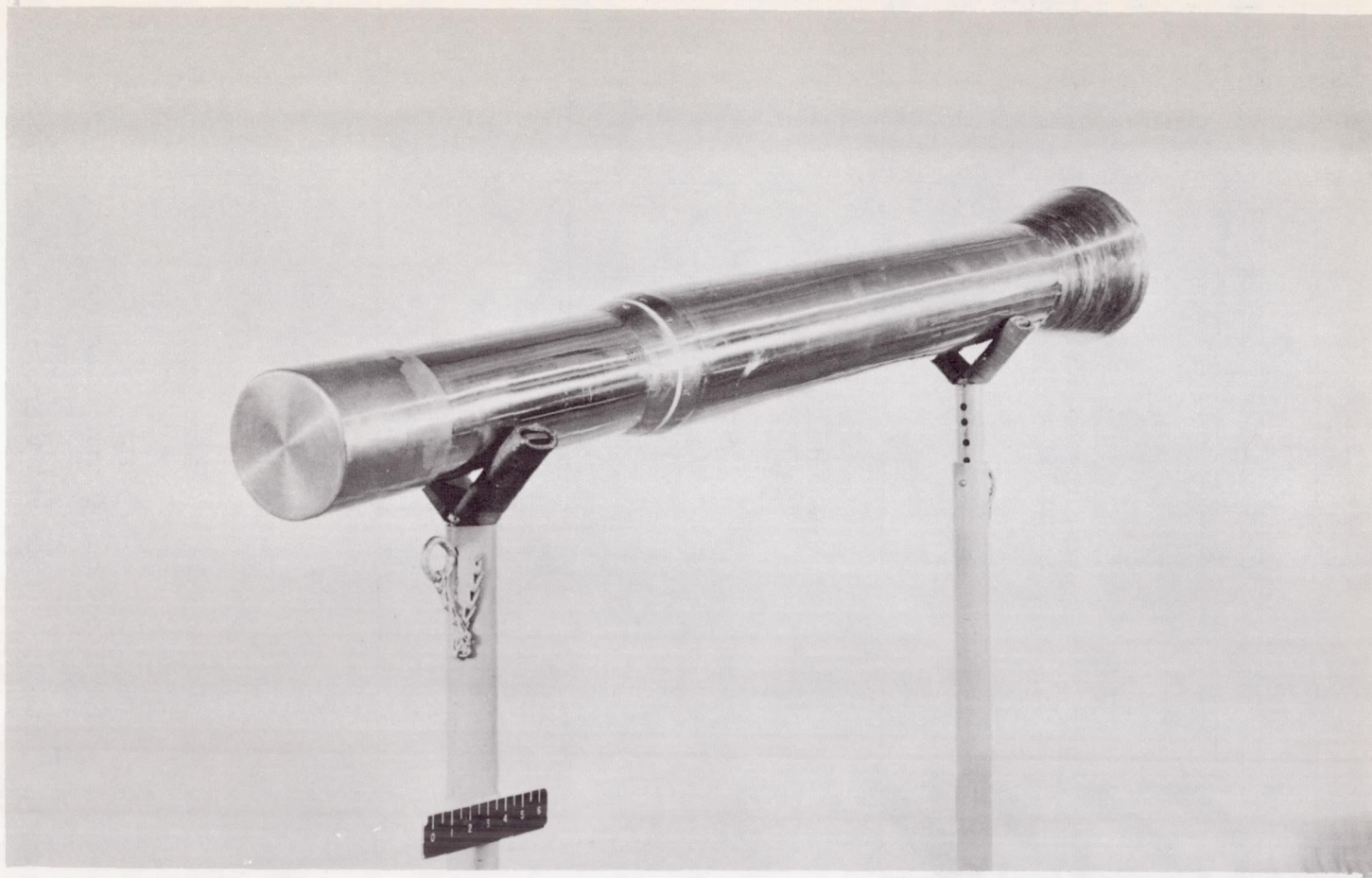
Figure 3.- Fifth stage of five-stage rocket showing nose shape tested.   L-95097.1
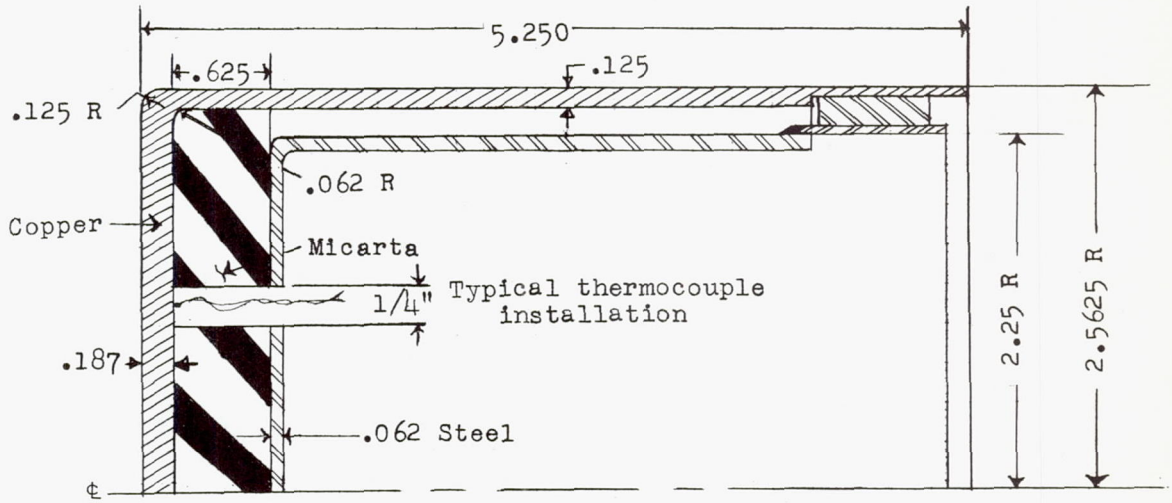
(a) Nose detail.
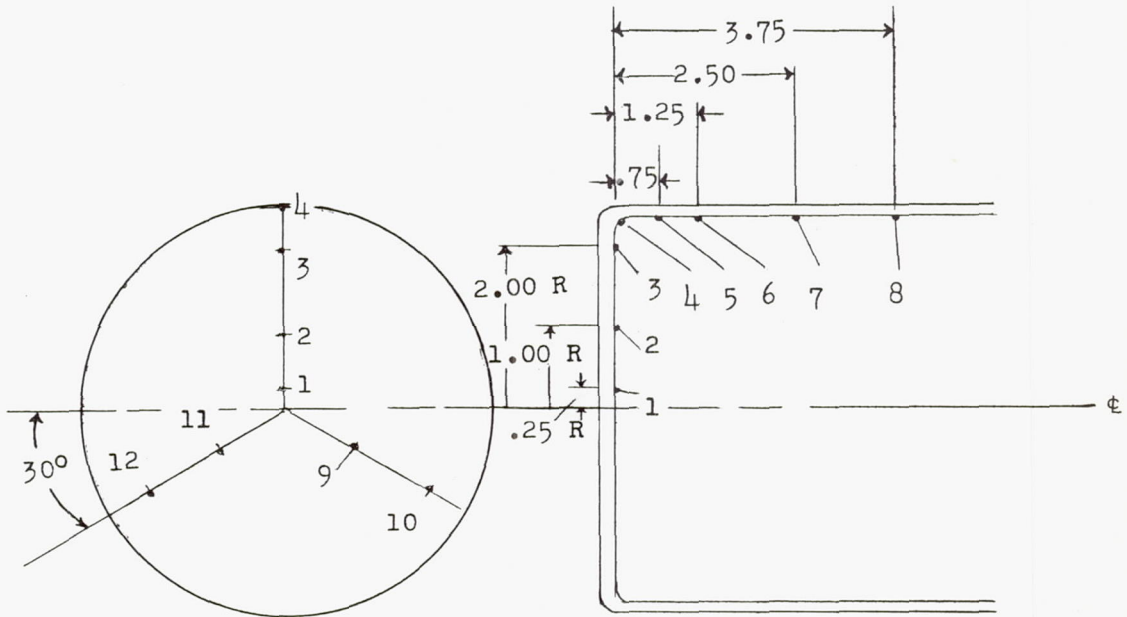
(b) Location of thermocouples.

Figure 4.- Details of nose and thermocouple installation.
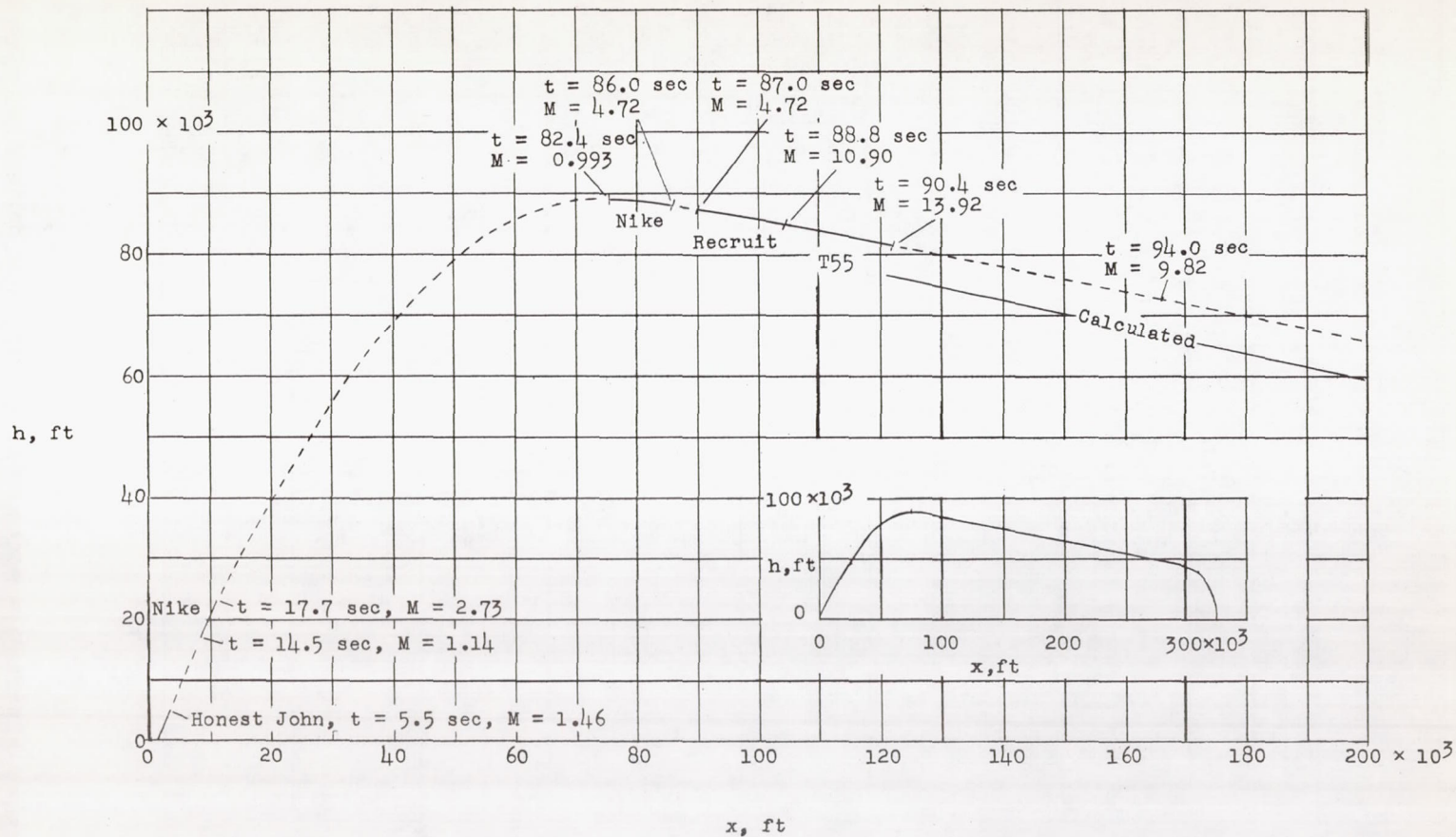
Figure 5.- Model trajectory.
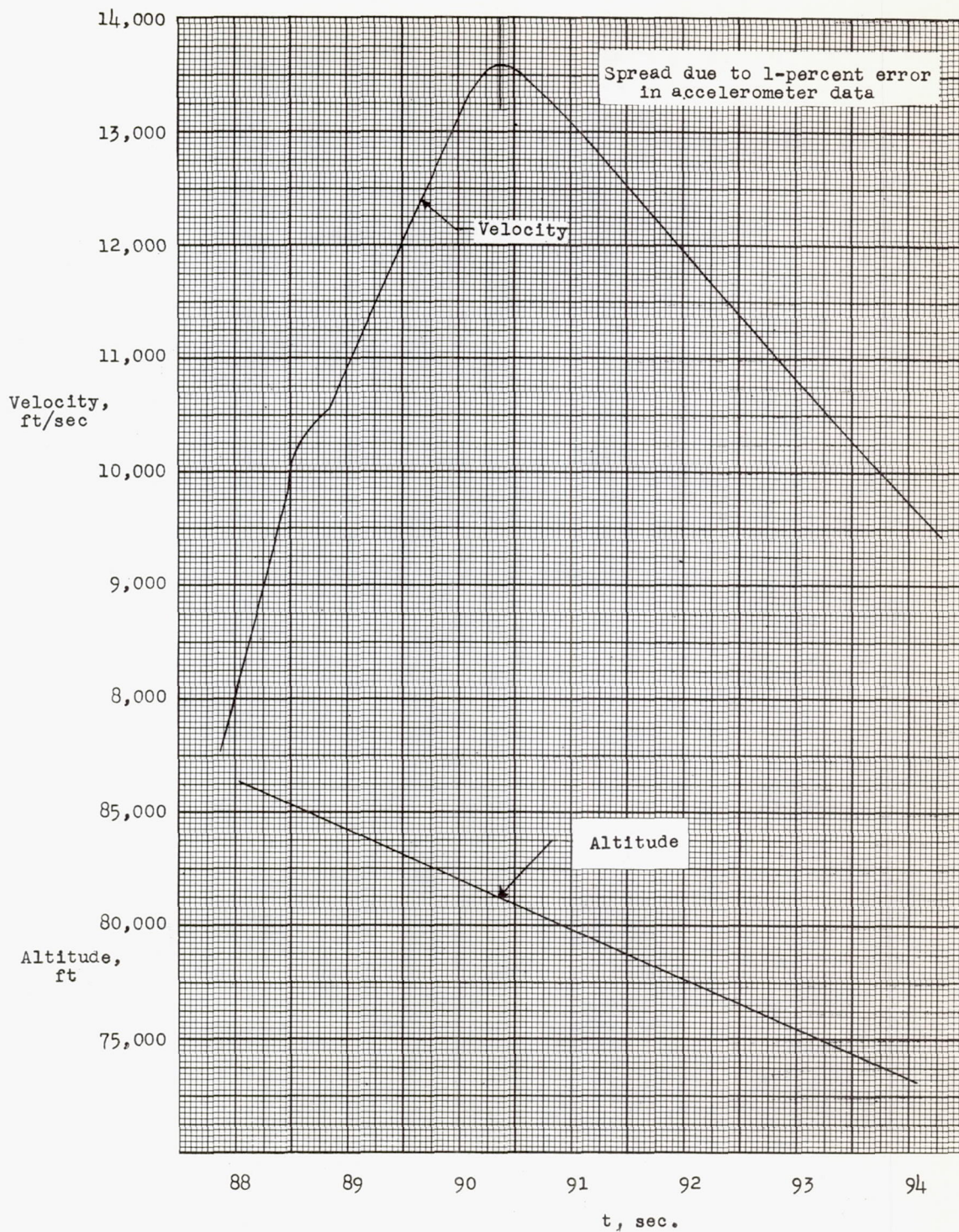
Figure 6.- Model velocity and altitude history.
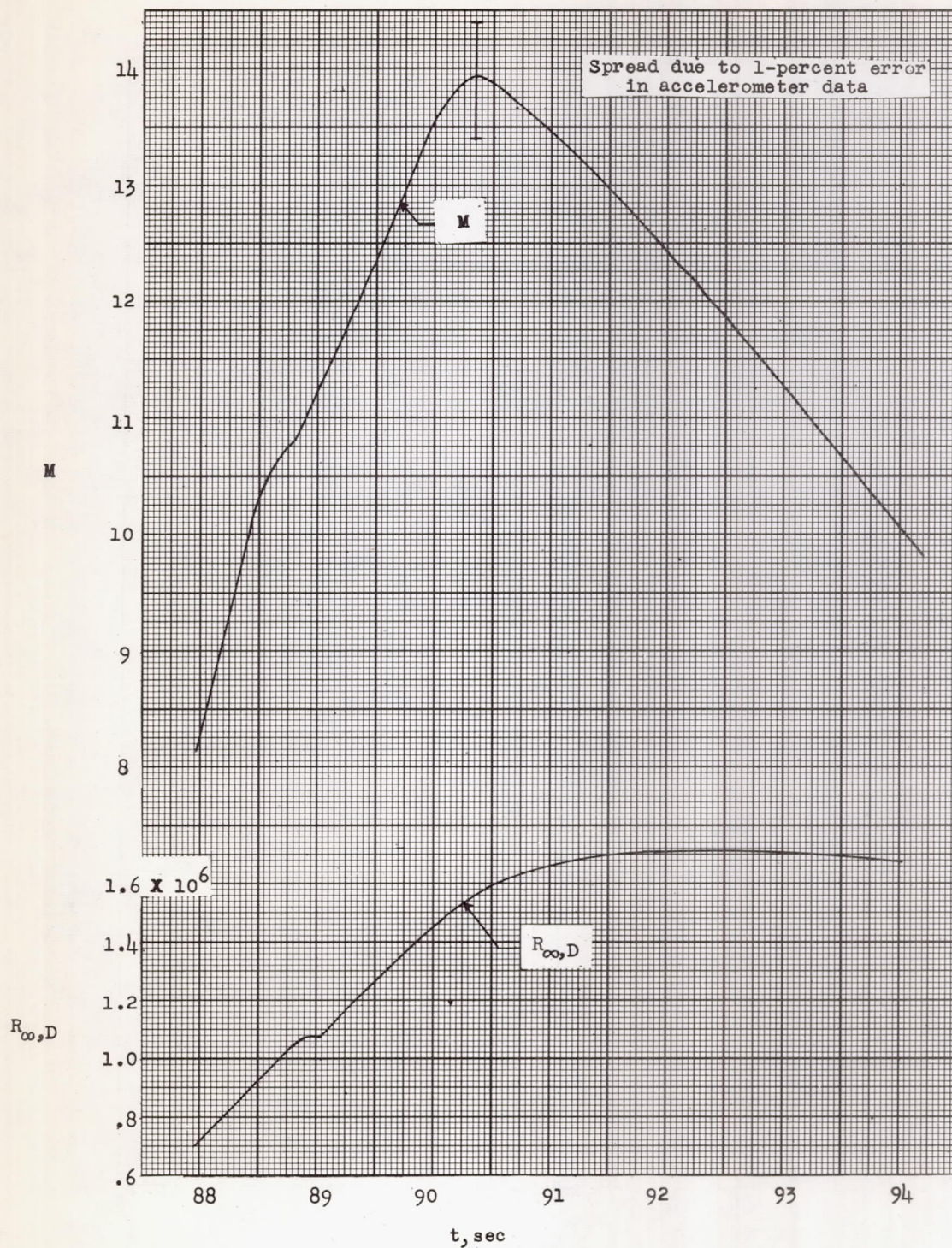
Figure 7.- Model Mach number and Reynolds number history.
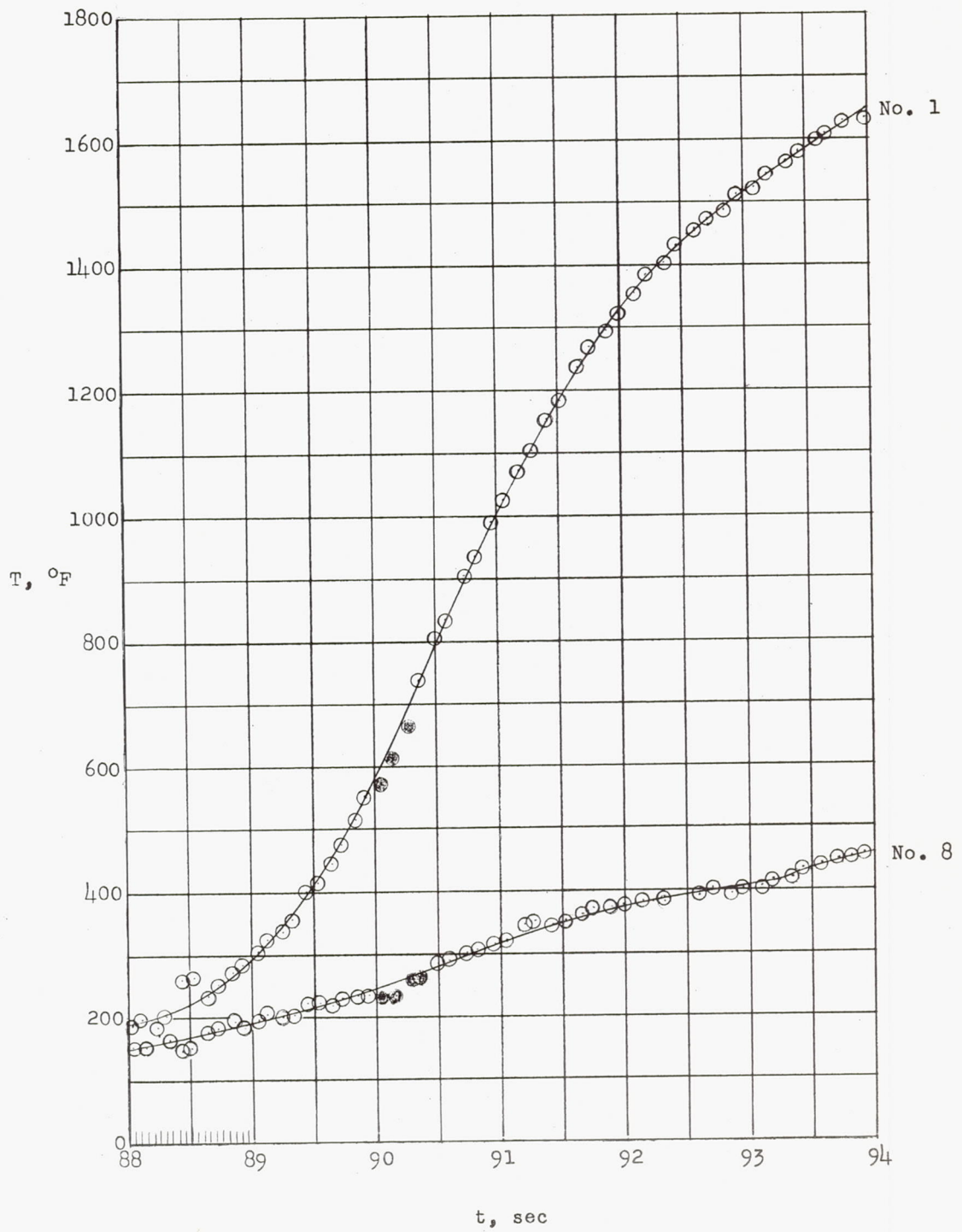
Figure 8.- Typical variation of temperature with time.

Figure 9.- Apparent heating rates compared with values corrected for lateral heat flow.
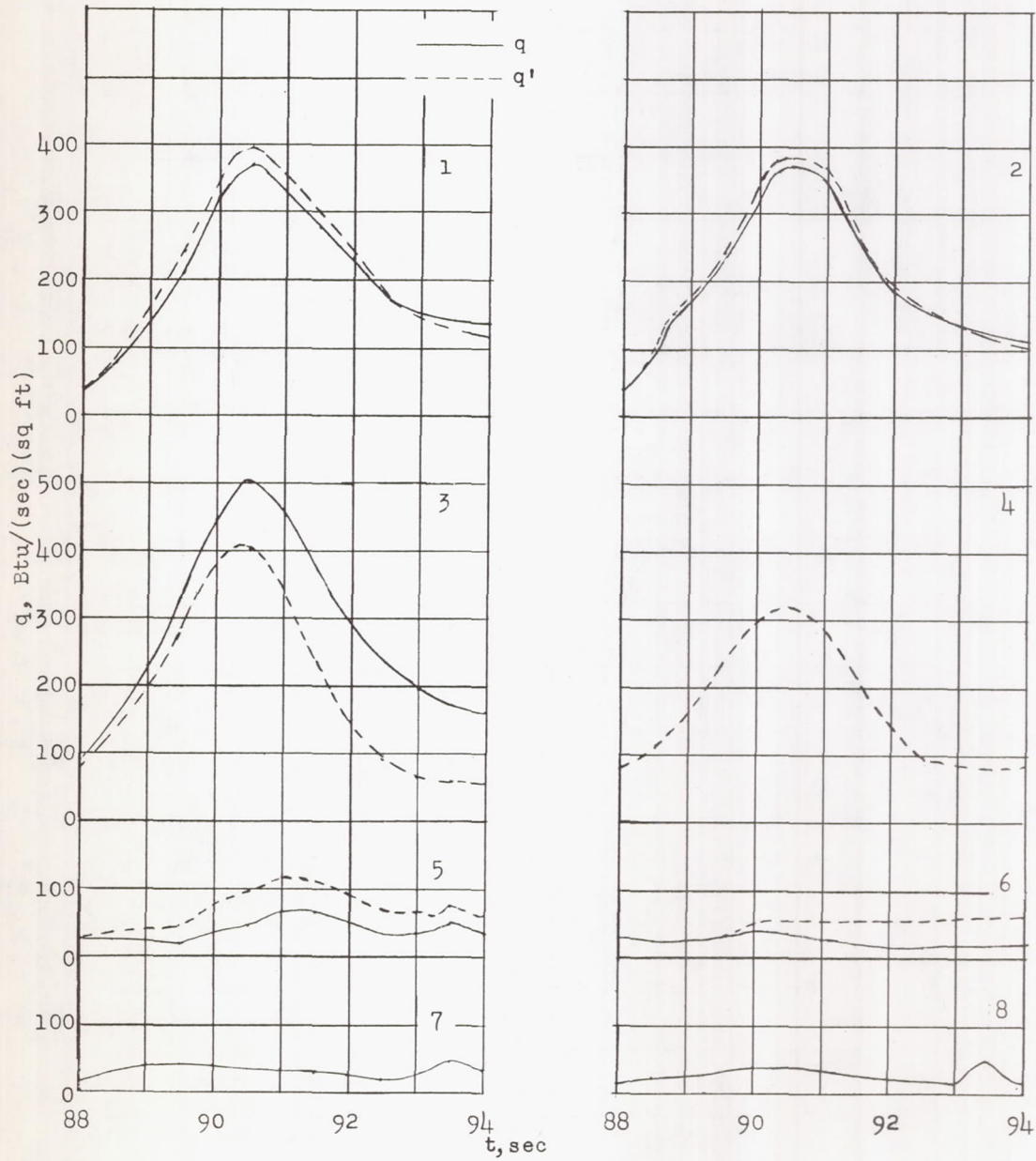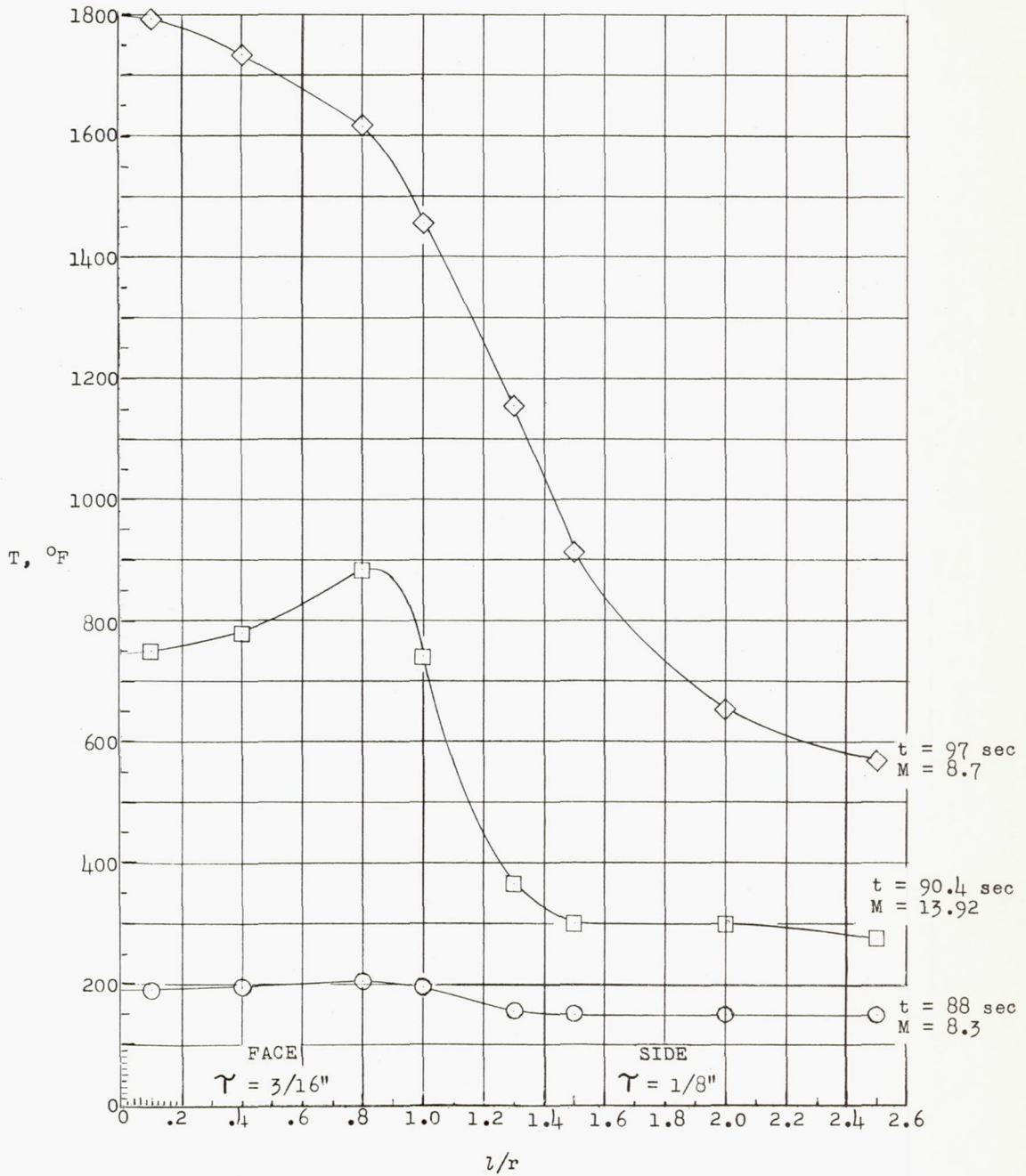
Figure 10.- Temperature as function of position on nose.
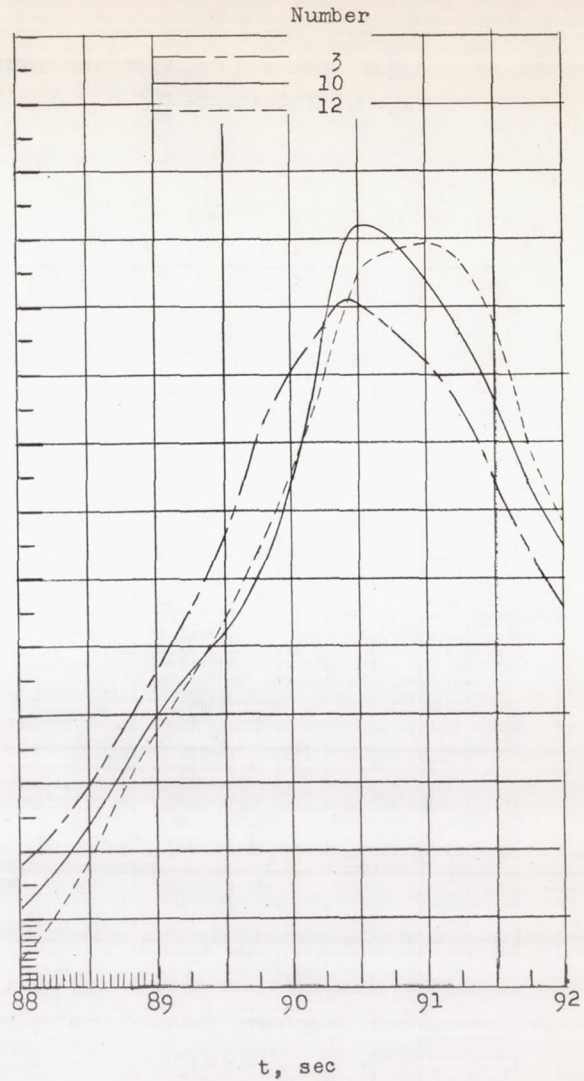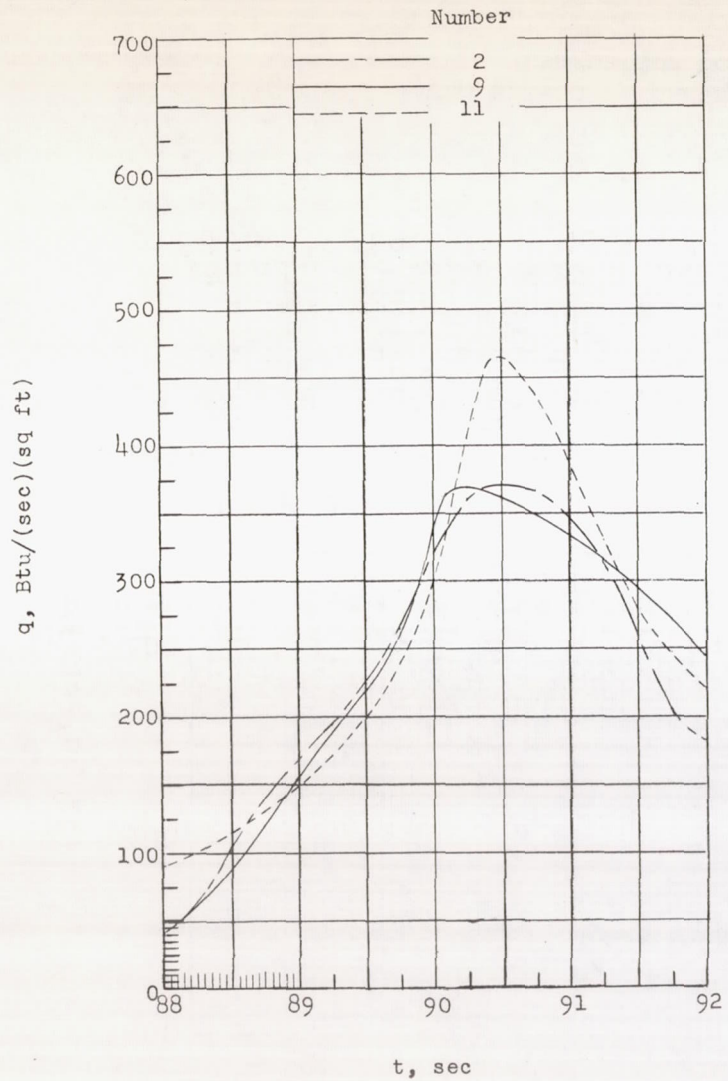
Figure 11.- Comparison of heating rates measured at three radial locations on the flat face.
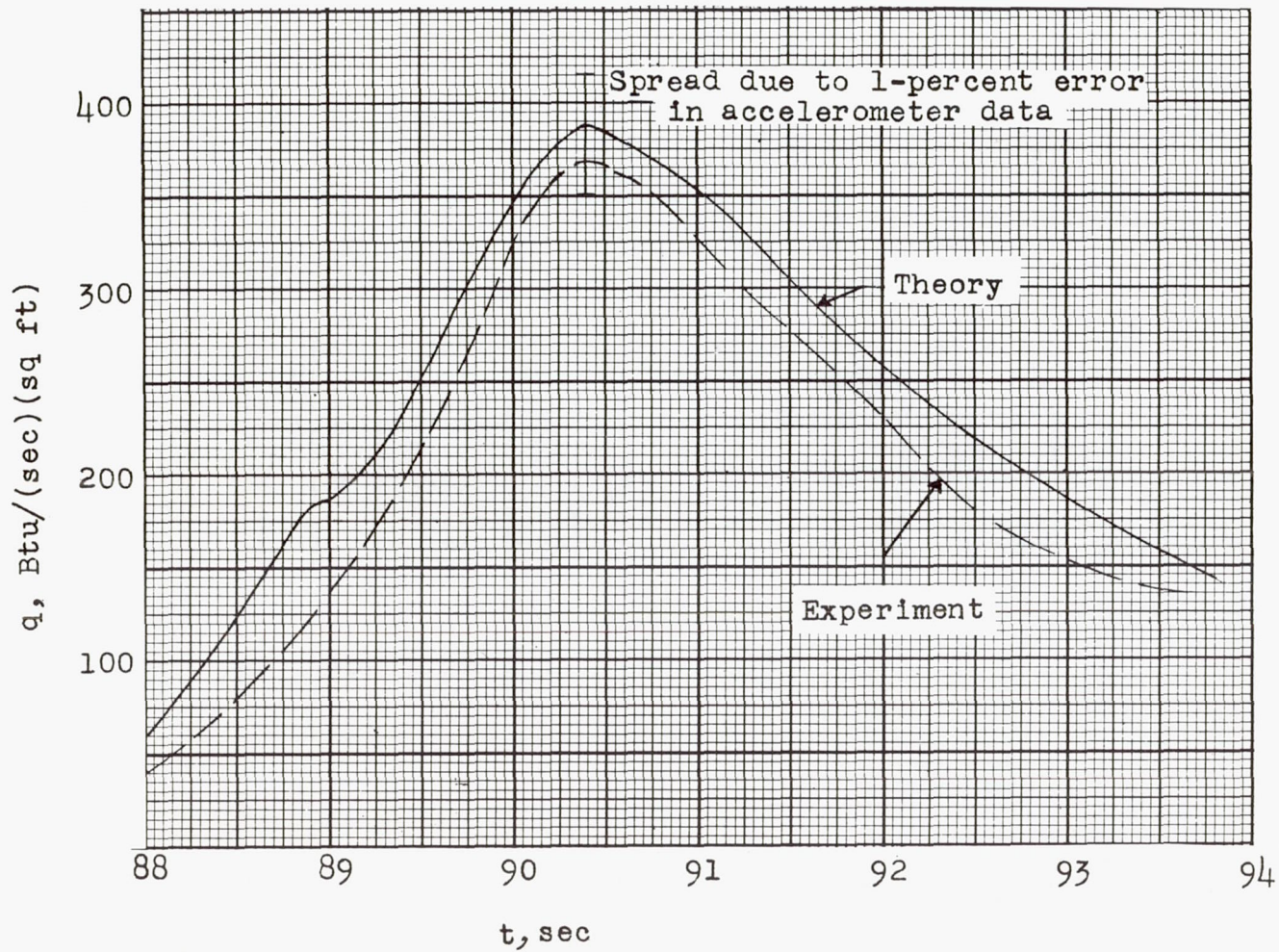
Figure 12.- Comparison of theoretical and measured heating rates at stagnation point (thermocouple 1).
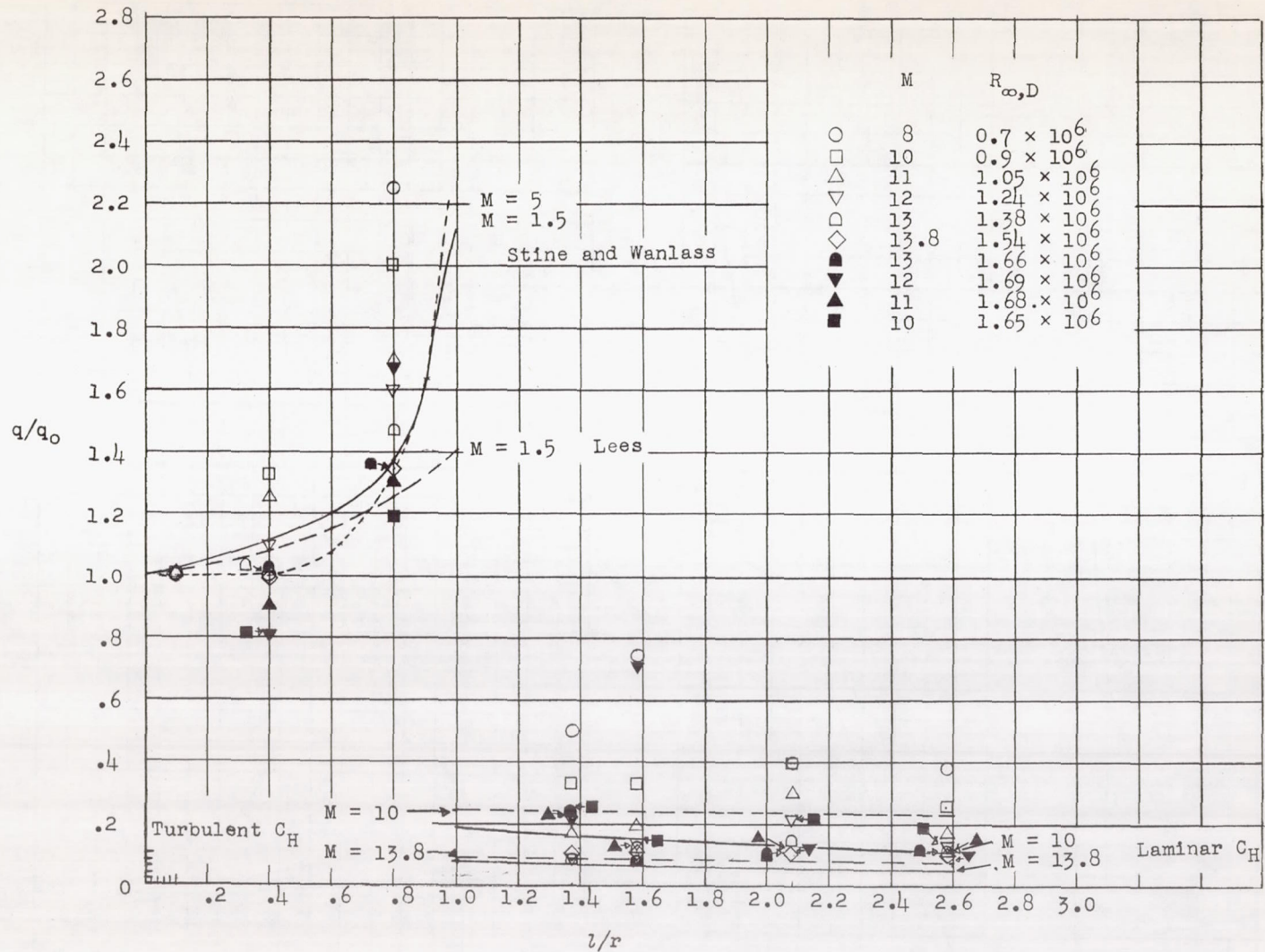
Figure 13.- Comparison of measured and theoretical ratios of local heating rates to stagnation heating rates.
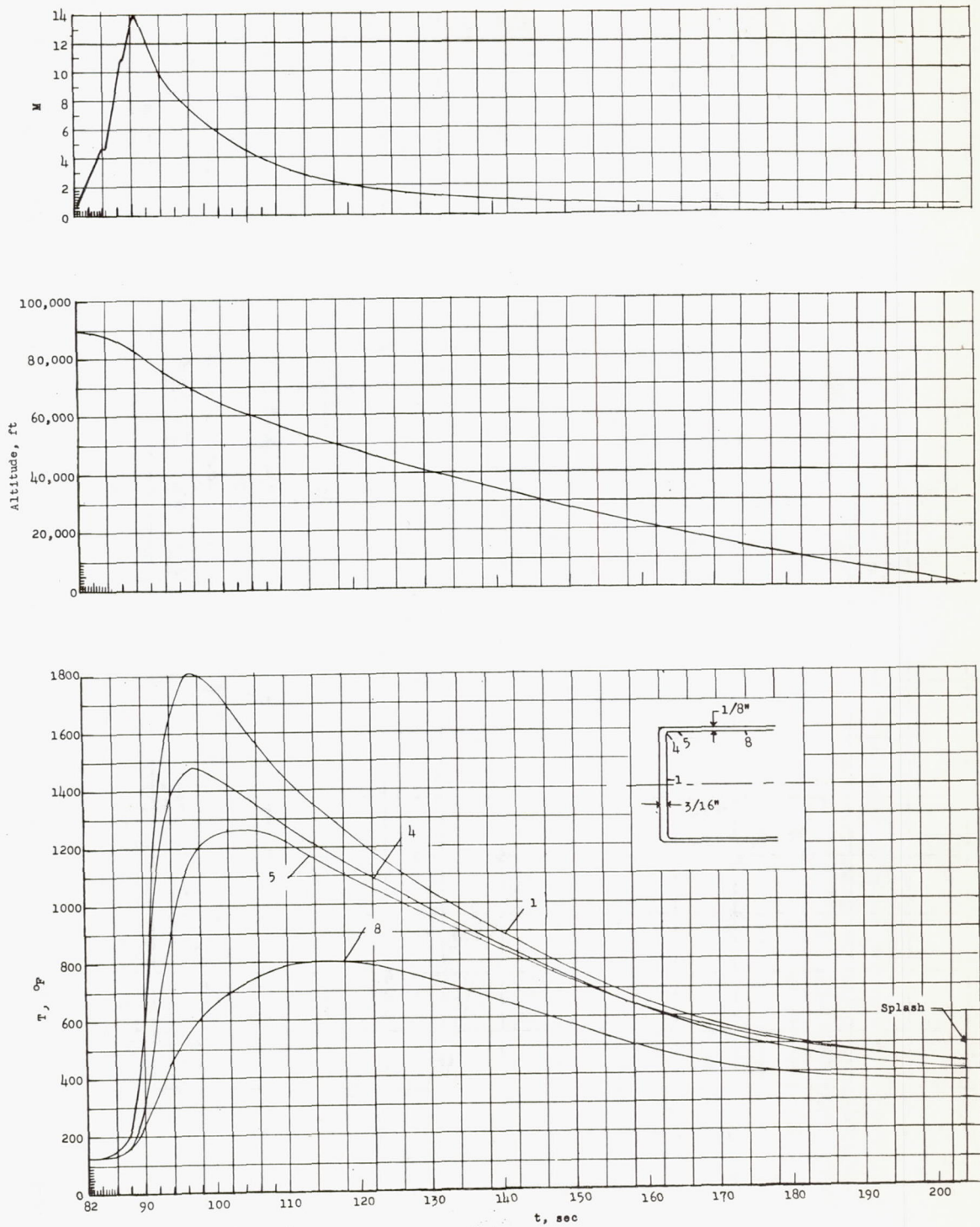
Figure 14.- Variation of Mach number, altitude, and temperatures with time from beginning of reentry until splash.
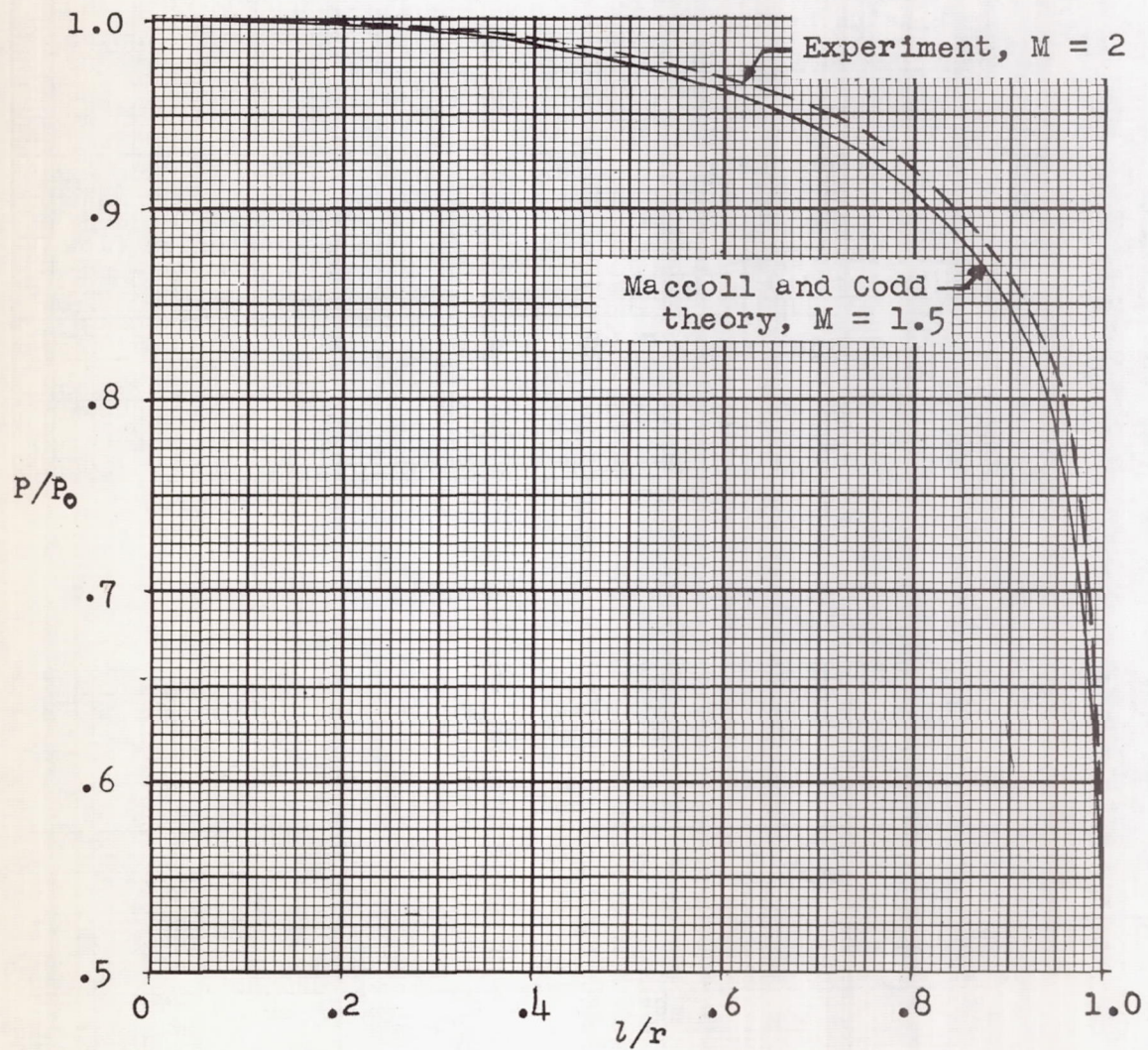
Figure 15.- Flat-face pressure distributions.

$$\frac{D}{U_\infty}\left(\frac{dU}{dx}\right)_o$$

Sphere

Blasius hemisphere

Hemisphere experimental (Korobkin)

Newtonian flow

Flat face (Probstein)

Flat face: $\frac{r}{a_o}\left(\frac{dU}{dx}\right)_o = 0.3$

M

(a) Velocity gradients.

$$\frac{q_{o,f}}{q_{o,h}}$$

Incompressible solution (Probstein)

$\frac{r}{a_o}\left(\frac{dU}{dx}\right)_o = 0.3$

M
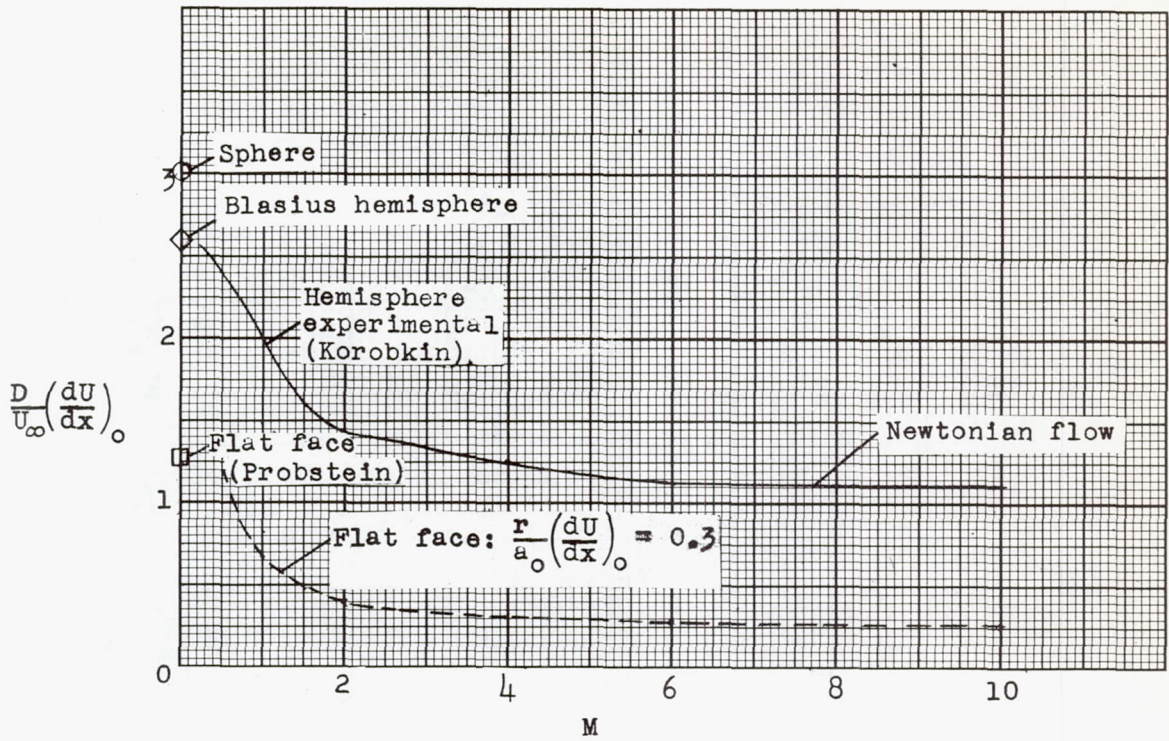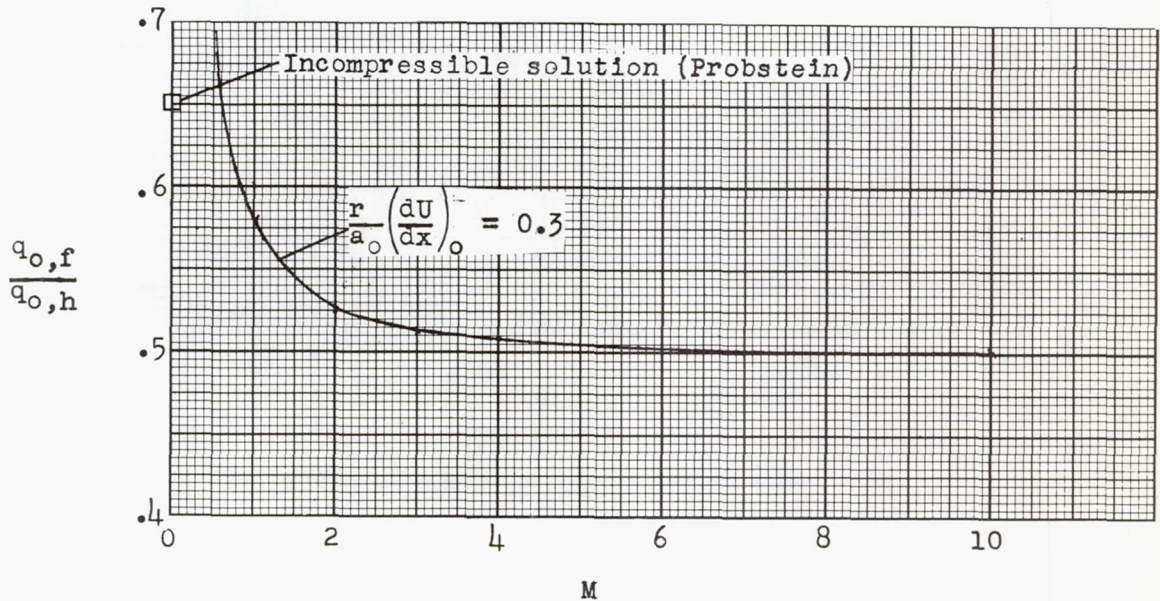
(b) Heat-transfer rates.

Figure 16.- Comparison of flat and hemispherical stagnation-point velocity
gradients and heat-transfer rates.